Cell Tissue Res (1994) 277:391–400

Cell & Tissue Research

Endocardial endothelium in the rat: junctional organization and permeability

L. J. Andries, D. L. Brutsaert
Department of Physiology, University of Antwerp, Groenenborgerlaan 171, B-2020 Antwerp, Belgium

Received:17 March 1992 / Accepted: 2 February 1994

Abstract. Selective permeability of endocardial endothelium has been suggested as a mechanism underlying the modulation of the performance of subjacent myocardium. In this study, we characterized the organization and permeability of junctional complexes in ventricular endocardial endothelium in rat heart. The length of intercellular clefts viewed en face per unit endothelial cell surface area was lower, and intercellular clefts were deeper in endocardial endothelium than in myocardial vascular endothelium, whereas tight junctions had a similar structure in both endothelia. On this basis, endocardial endothelium might be less permeable than capillary endothelium. However, confocal scanning laser microscopy showed that intravenously injected dextran 10000 coupled to Lucifer Yellow penetrated first the endocardial endothelium and later the myocardial capillary endothelium. Penetration of dextran 10000 in myocardium occurred earlier through subepicardial capillary endothelium than through subendocardial capillary endothelium. Penetration of tracer might thus be influenced by hydrostatic pressure. Dextran of MW 40000 did not diffuse through either endocardial endothelium or capillary endothelium. The ultrastructure of endocardial endothelium may constitute an adaptation to limit diffusion driven by high hydrostatic pressure in the heart. Differences in paracellular diffusion of dextran 10000, between endocardial endothelium and myocardial vessels, may result from differing permeability properties of the endocardium and underlying myocardium.

Key words: Heart – Endocardial endothelium – Capillary endothelium – Myocardium –Permeability – Tight junctions – Dextran – Confocal scanning laser microscopy – Rat (Wistar)

Correspondence to: L. J. Andries

Introduction

Vascular endothelium forms a selectively permeable barrier to the diffusion of molecules (Pappenheimer et al. 1951; Ward et al. 1988). The zonula occludens or tight junction is an important determinant of this transendothelial permeability. Like epithelial tissues, monolayers of cultured endothelium establish a transcellular electrical resistance and express ZO-1, a tight junction-associated protein (Li and Poznansky 1990). Vascular endothelial cells have a junctional complex consisting of a tight junction and an adherent junction which is associated with a peripheral band of actin filaments (Gotlieb et al. 1991; Bundgaard 1980, 1984; Gabbiani et al. 1975). Both the tight junctions and the peripheral actin band participate in the control of transendothelial permeability in cultured endothelial cells (Schnittler et al. 1990; Alexander et al. 1988; Shasby et al. 1982)

Considerable differences exist in the organization of tight junctions and in transendothelial permeability between vascular endothelia of different organs (Jain 1987) as well as between segments of a given vascular unit (arteriole, capillary or venule) within the same organ (Simionescu et al. 1975). For example, the low transendothelial permeability of capillaries forming the blood-brain barrier has been ascribed to the continuous belt of tight junctions, with negative charges at the luminal surface, and to the small number of transport vesicles (Cervos-Navarro et al. 1988). By contrast in myocardial capillaries, tight junctions exhibit some discrete discontinuities (Bundgaard 1984) and are more permeable than capillaries of the blood-brain barrier (Ward et al. 1988). Very leaky junctions have been found in endothelium of postcapillary venules; these vessels have discontinuous tight junctions (Simionescu et al. 1975) and allow leakage of macromolecules after application of inflammatory mediators (Svensjö and Grega 1986).

Endocardial endothelium (EE), another continuous endothelium, has recently been shown to modulate the performance of the subjacent myocardium (Brutsaert et al. 1988, Brutsaert 1989, Brutsaert and Andries 1992).

Both release of inotropic substances (Brutsaert 1989; Smith et al. 1991; Schulz et al. 1991) and/or a trans-EE electrochemical control (Brutsaert 1989) have been proposed as possible mechanisms. A trans-EE electrochemical control would depend upon the degree of leakiness of the endothelium. The complex interdigitations and extensive overlap of the junctional cell edges in EE (Melax and Leeson 1967; Anversa et al. 1975) and the presence of tight junctions similar to those of myocardial capillaries (Anversa et al. 1975), suggest that EE might have unique permeability properties. Structural features other than the arrangement of tight junctions play an important role in paracellular permeability (Bundgaard and Frøkjaer-Jensen 1982). These include the average width of the intercellular clefts and cleft length per unit surface area of the endothelial cells, and the average depth of the clefts (Fig. 1).

To investigate whether and to what extent the permeability of EE differs from that of vascular endothelium, we compared the structure of junctional regions of EE and myocardial capillaries in rat heart with transmission electron microscopy and confocal scanning laser microscopy (CSLM), and investigated the permeability of the EE and capillaries by use of intravenously injected dextrans coupled to Lucifer Yellow and CSLM.

Materials and methods

Experiments on rats were performed in accordance with the "Principles of Laboratory Animal Care" (NIH publication No. 85–23, revised 1985) and with the "Belgian Law on the Protection of Animals". For transmission electron microscopy, 7 Wistar rats (100–200 g) were used. Rats were deeply anaesthetized with Hypnorm (Janssen Pharmaceutica, Beerse, Belgium). The hearts were removed, rinsed (30s to 1 min, until all blood was pumped out of the ventricle) in Krebs-Ringer solution and then fixed by immersion in 2.5% (v/v) glutaraldehyde in PIPES-HEPES buffer (Mg acetate 2 mM, KCl 5 mM, NaCl 15 mM, PIPES 60 mM, HEPES 25 mM, pH 7.0) or in 0.1 M sodium cacodylate buffer at room temperature. The ventricles were opened just below the atria and fixative solution was injected into the right and left ventricular lumen. After fixation for 15 to 60 min, small samples were excised from the right and left ventricles, refixed for at least 1 h, postfixed in 0.5% (w/v) osmium tetroxide in 0.1 M cacodylate buffer for 1 h and then rinsed in cacodylate buffer. Most tissue blocks were further treated for 1 h with 0.2% (w/v) tannic acid (MW 1701, Polysciences, Eppelheim, Germany) in cacodylate buffer. All tissue blocks were stained en bloc with 1% (w/v) uranyl acetate in distilled water, then dehydrated and embedded in Epon. Serial ultrathin sections with gray to silver color were stained with 25% (w/v) uranyl acetate in methanol and lead citrate (Reynolds 1963). From some preparations, a series of 20 to 25 consecutive sections, with a thickness of 40–50 nm, could be obtained. The sections were examined by use of a Jeol 100-B electron microscope operated at 60 kV. The depth of the intercellular clefts was estimated as described by Bundgaard and Frøkjaer-Jensen (1982). Only straight sectioned "simple" clefts were selected and depth was measured from the luminal to the abluminal end. Complex intercellular regions with interdigitations and overlapping edges were not included.

Confocal scanning laser microscopy (CSLM) of EE stained with Bodipy-Phallacidin was used to visualize the cell borders of the EE; this allowed measurement of the length of the intercellular clefts per unit endothelial cell surface area. Rats ($n = 5$) anaesthetized with Hypnorm (Janssen Pharmaceutica, Beerse, Belgium) were fixed by retrograde perfusion by a cannula in the abdominal aorta for 5 min with 4% freshly prepared formaldehyde in a HEPES buffer ($CaCl_2.2H_2O$, 1.2 mM, $MgCl_2.6H_2O$, 0.5 mM, KCl 2.7 mM, KH_2PO_4 1.5 mM, NaCl 136.9 mM, $NaH_2PO_4.H_2O$ 8.1 mM, HEPES 25.0 mM, D-glucose 5.0 mM, pH 7.2). The heart was excised and fixed for a further 25 min. Tissue samples were dissected from following areas in left and right ventricle: papillary muscles (usually the whole muscle), lateral wall, septum (including atrioventricular valve), outflow tract, myocardial microvessels, and in addition: thoracic aorta. After permeabilization in 0.1% (v/v) Triton X-100 for 20 s, tissue blocks were immersed in 0.1 M glycine for 10 min. The specimens were stained for 20 min with 3.3×10^{-6} M Bodipy-phallacidin (Molecular Probes, Eugene, USA). Strips with a thickness of about 0.2 to 1.0 mm were cut parallel to the endocardial surface of the stained tissue blocks, mounted in small chambers on a slide filled with Slowfade (Molecular Probes, Eugene, USA) and closed with a coverslip. En face optical sections through the EE were made with the Biorad MRC 600 using the FITC filter set (BHS) and a Leitz 100x oil-immersion objective. To determine the surface area of endothelial cells, morphometric analysis of the Biorad images was performed with Fenestra (Confocal Technology, Liverpool, UK). In en face views of EE, the length of intercellular clefts per unit en-

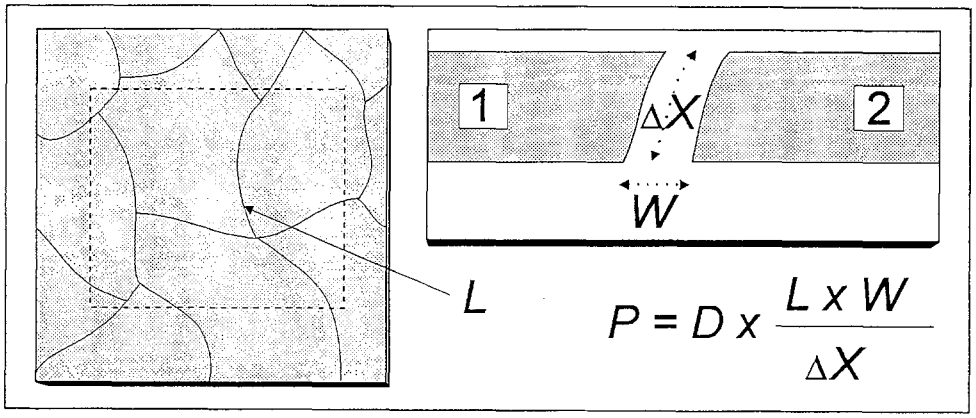

Fig. 1. Schematic drawing to illustrate the 3-dimensional parameters which determine permeability (P) through intercellular clefts of endocardial endothelium (EE). L is the average length of intercellular clefts per unit endothelial cell surface area determined from an en face view of EE. The upper right insert represents a perpendicular section through 2 EE cells (*1, 2*). W is the average width of the intercellular cleft, a parameter which can be influenced by the presence of junctions (not shown); ΔX is the average depth of the cleft from the luminal to the abluminal opening. L, W and X influence permeability with equal weight. D is the restricted diffusion coefficient of the solute. Modified after Bundgaard and Frøkjaer-Jensen (1982)

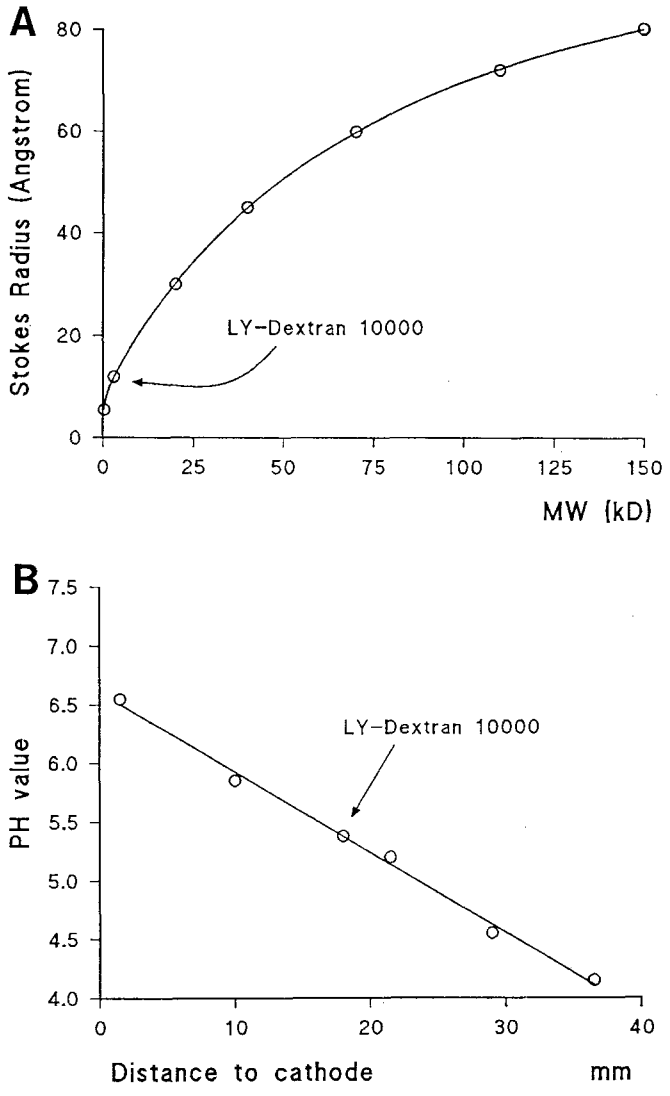

Fig. 2A, B. Physico-chemical properties of LY-dextran 10000. **A** Curve constructed by non-linear regression analysis of tabulated data of the molecular weight and Stokes radii of dextrans from Tervo et al. (1979) and Thorball (1981). $r^2 = 0.999976$; $y = (8.9*x)/(0.29+x) + (126.6*x)/(93.5 + x) - 0.046*x$. On this basis, the Stokes radius of LY-dextran 10000 is 20.4 Angström. **B** The isoelectric point (pI) of LY-Dextran 10000 was determined by isoelectric focusing, using the Phastsystem of Pharmacia LKB. The following standard markers were applied: human carbonic anhydrase B (pH:6.55); bovine carbonic anhydrase B (pH 5.85); β -lactoglobulin A (pH 5.20); soybean trypsin inhibitor (pH 4.55); glucose oxidase (pH 4.15). After Phastgel Silver Staining, the distances were measured between the cathode and the applied substances (markers and LY-dextran 10000). By regression analysis: PHvalue = 6.61 – 0.07 × Distance to Cathode, the pI of LY-dextran is 5.38

dothelial cell surface area was determined by measuring the length of the peripheral borders in a rectangular zone (Fig. 1).

To investigate EE permeability, dextrans of molecular weight 10000 or 40000 coupled to Lucifer Yellow (LY-dextrans) (Molecular Probes, Eugene, USA) were used. The molecular radius of the dextrans was interpolated from tabulated data of Tervo et al. (1979) and Thorball (1981). By applying non-linear regression of these data, a value of 2.0 nm was derived for LY-dextran 10000 and 4.5 nm for LY-dextran 40000 (Fig. 2 A). According to the manufacturer, the LY-dextrans have one-half to two dyes per dextran in the 10000 MW range and two to four dyes in the 40000 MW range; the net charge of the conjugate (theoretical isoelectric point: 5.5) is negative by the anionic Lucifer Yellow. By isoelectric focussing, the isoelectric point of LY-dextran 10000 measured 5.4 (Fig. 2 B). LY-dextrans have the advantage that, by the addition of lysine residues, they can be fixed with formaldehyde and glutaraldehyde (Gimlich and Braun 1985). We cannot exclude that in vivo part of the LY-dextrans interacts with plasma proteins and that such protein binding might influence the rate of leakage through endothelium.

The LY-dextrans (100–200 mg/kg body weight) were dissolved in 0.25 ml Krebs-Ringer solution and injected over 5 s via a cannula in the jugular vein in anaesthetized (Hypnorm, Janssen Pharmaceutica, Beerse, Belgium) Wistar rats ($n = 27$) weighing 100 gm. For comparison, 4 animals were injected with 12.5 mg unbound Lucifer Yellow (MW 457; Molecular Probes, Eugene, USA) dissolved in 0.25 ml Krebs-Ringer solution. Hearts were then excised and fixed by immersion in 2% formaldehyde freshly prepared from paraformaldehyde, and 1% glutaraldehyde in Millonig buffer after intervals of 60 s, 90 s, 120 s, 5 min, 10 min and 30 min. Included in these periods was the time needed for excising (10 to 15 s) and subsequent rinsing (5 s) in Krebs solution, at room temperature. The ventricles were opened and specimens were dissected and further fixed for 2 h. Five hearts were fixed with 4% freshly prepared formaldehyde in Millonig buffer (pH 7.2). After 20 min, the tissue blocks were further fixed by immersion overnight in 4% formaldehyde in sodium borate (pH 10). The latter procedure offers an adequate fixation (Berod et al. 1981) and a lower degree of autofluorescence in myocardial tissue, compared to glutaraldehyde-fixed tissue. For confocal scanning laser microscopy, some tissue blocks were stained with propidium iodide. Strips with a thickness of about 0.2 to 1.0 mm were cut from the tissue blocks parallel to the endocardial surface, mounted in Histofluor on a slide, and observed with the Biorad MRC 600 microscope. For epifluorescence microscopy, tissue blocks were dehydrated with ethanol and embedded in Historesin (Cambridge Instruments, Heidelberg, Gemany). Semithin sections were cut on a pyramitome with glass knives and observed by use of a Zeiss Jung epifluorescence microscope equipped with FITC filters.

Results

Structure of intercelullar borders in endocardial endothelium

In EE of left and right ventricle ($n = 7$) peripheral parts of two or more EE cells frequently formed complex interdigitations with considerable overlap between cells (Fig. 3 A). Other intercellular junctions had a somewhat more simple structure with straight intercellular clefts between two adjacent cells (Fig. 3 B, C).

After tannic acid treatment the apical membrane surface of EE cells, including the membrane of luminal vesicles and the content of many apparently cytoplasmic vesicles, was delineated by a thick layer of stained material (Fig. 3 A, B). Transendothelial channels formed by single or fused vesicles were not observed. The cell coat at the apical part of most intercellular clefts was also stained by tannic acid. Penetration of tannic acid into the intercellular clefts was usually interrupted at punctate junctional contacts. Consecutive sections demonstrated the presence of 1 or 2 punctate junctional contacts (Fig. 3 B,C), which is in agreement with previous ultrastructural investigations (Anversa et al. 1973, 1975; Turcotte et al. 1982). No dense staining of the cell coat, after treatment with tannic acid, was observed beyond the level of these junctional contact points. However, in 4 out of 170 sec-

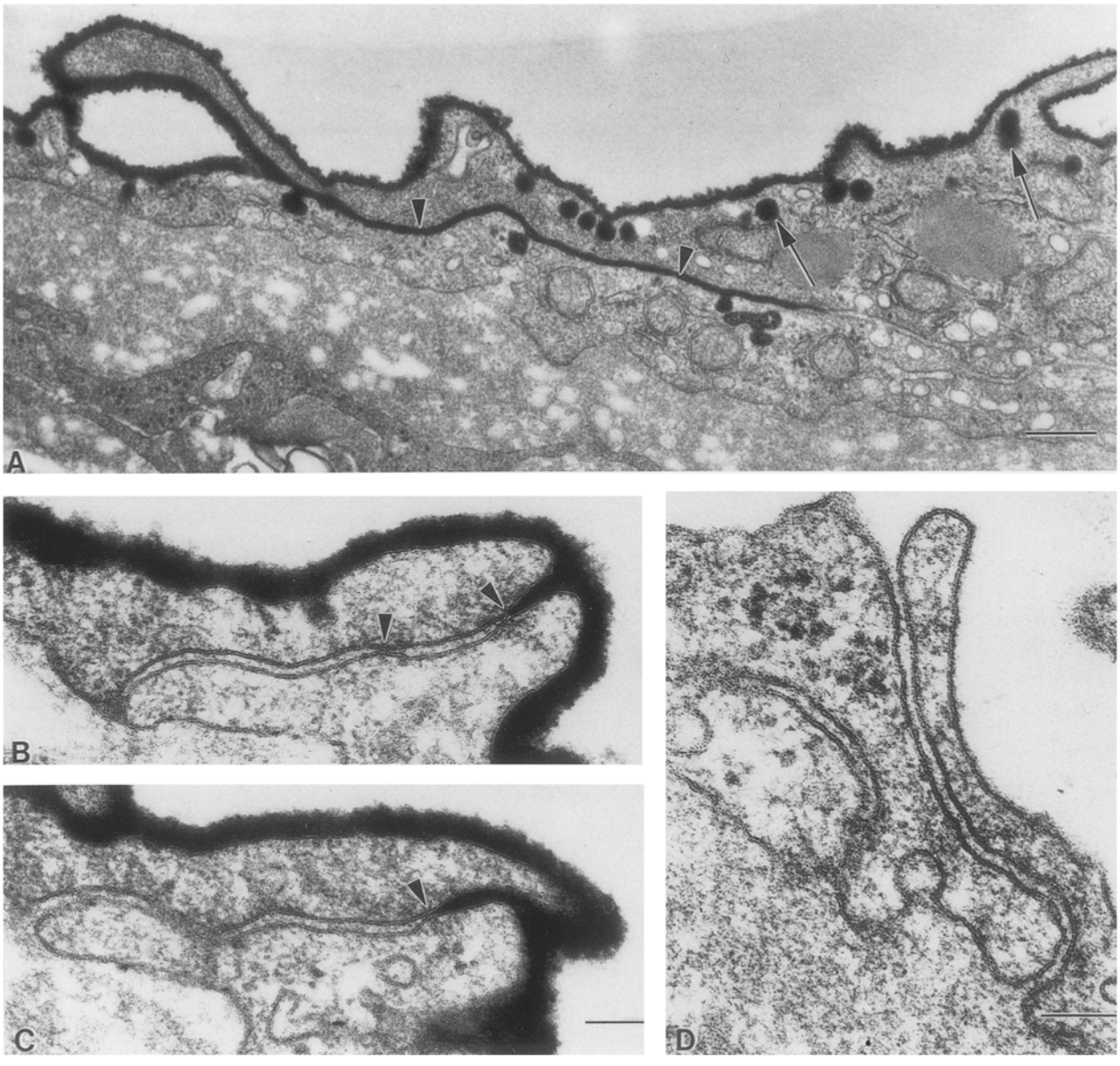

Fig. 3A–D. Transmission electron micrographs of junctional areas of EE from rat left ventricle. **A** Junctional area with extensive cellular overlap. The cell coat of the apical surface including that of apparent cytoplasmic vesicles (*arrows*), and part of the intercellular cleft (*arrowhead*) is densely stained by tannic acid. *Scale bar*: 250 nm. **B, C** Micrographs of 2 sections from a series of consecutive ultrathin sections showing an intercellular cleft between 2 EE cells. The cell coat of the apical surface is well stained. Penetration of tannic acid in the intercellular cleft stopped at the first punctate junctional contact. **B** Tight junction formed by 2 obliterating points (*arrowheads*) in the intercellular cleft. **C** A single contact point (*arrowhead*) obliterates the intercellular cleft. *Scale bar*: 100 nm. **D** Junctional area between 2 EE cells with open intercellular cleft. *Scale bar*: 100 nm

tioned intercellular clefts, intercellular clefts were free of junctions (Fig. 3 C). No qualitative differences in ultrastructural organization of the intercellular clefts were noticed between the left and right ventricle.

The mean depth of the less complex and perpendicularly sectioned intercellular contact areas (such as in Fig. 3 B, C), from luminal to abluminal cleft opening in EE was significantly larger than that of the clefts between endothelial cells of myocardial capillaries (Fig. 4 A). Because complex junctional intercellular clefts with interdigitations and overlapping cell parts were not included, the quoted depth of intercellular clefts underestimates the true depth of the intercellular clefts.

Using CSLM and Bodipy-phallacidin staining, which predominantly labels F-actin at the peripheral borders of EE cells, the surface area of EE cells and the length of the intercellular clefts could be calculated. EE cells usually have a large surface area (Fig. 5 A, B, D) and hence the ratio length of intercellular clefts per square micrometer of endothelial cell surface area is low (Fig. 4 B). Endothelial cells of the atrioventricular valves (Fig. 5 D), microvascular endothelial cells (Fig. 5 C) and aortic endothelial cells have a smaller surface area and consequently a higher value for length of intercellular clefts per unit area (Fig. 4 B).

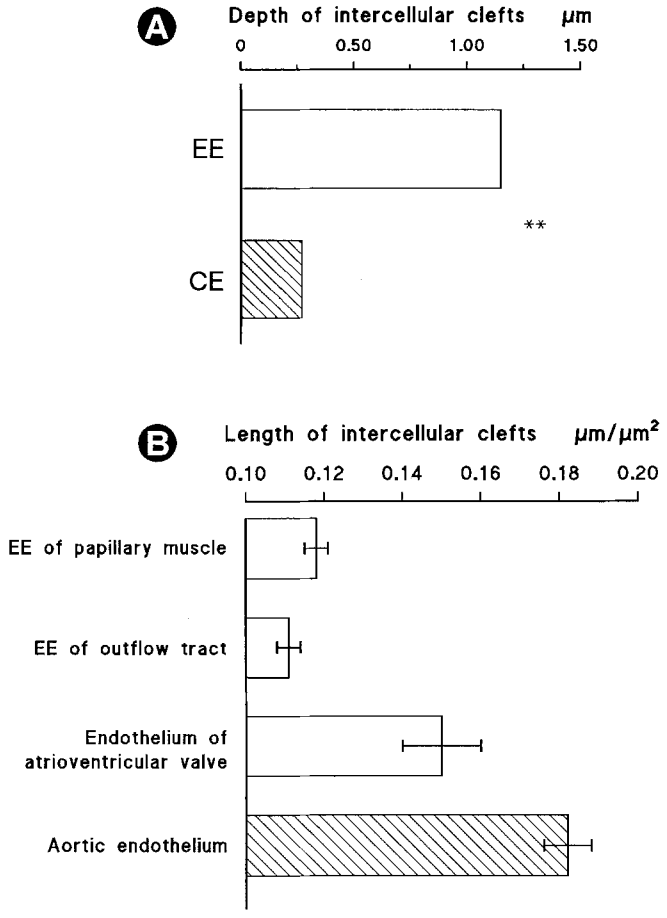

Fig. 4. **A** Harmonic mean values of depth of intercellular clefts in endocardial endothelium (*EE*) and endothelium of myocardial capillaries (*CE*) of left ventricle, observed by transmission electron microscopy. Only intercellular clefts of EE without extensive interdigitations and with perpendicularly cut cell membranes were included. (** $P \ll 0.01$; Mann-Whitney U-test). For comparison, the arithmetic mean ± S.E.M. of the depth of intercellular clefts is 1.49 ± 0.26 µm in EE and 0.53 ± 0.13 µm in endothelium of myocardial capillaries. **B** Average intercellular cleft length per µm² in different regions of EE, valvular endothelium and aortic endothelium

In vivo injection of dextrans coupled to Lucifer Yellow

In rat hearts fixed 60 *s* ($n = 3$) after intravenous injection of 25 mg of LY-dextrans with molecular weight of 10000, the tracer was confined to the coronary circulation in both ventricles. In the subendocardial interstitial tissue and in connective tissue of the myocardium, no tracer was observed with confocal scanning laser microscopy (Fig. 6 A). Within 90 *s* ($n = 4$), LY-dextrans 10000 penetrated into the EE in dispersed areas of the walls of the left and right ventricles, and stained the subendothelial connective tissue as discrete lines (Fig. 6 B); in the myocardium, the tracer remained confined to the coronary vessels (Fig. 6 B). *Two min* after injection ($n = 4$), LY-dextran 10000 penetrated deeper into the endocardial connective tissue (Fig. 6 C, D) thereby outlining large areas of the endocardial surface of the left and right ventricle. In the myocardium, LY-dextran 10000 was still not detected outside the coronary vessels. *Five min* after injection ($n = 4$), in optical sections transverse to the luminal surface of left and right ventricle, the endocardium was well stained and tracer was found in the extracellular space between the first and the second layer of myocytes in the subendocardial myocardium (Fig. 6 E), while extracellular spaces deeper into the subendocardial myocardium were unstained. Optical sections tangential to the luminal surface demonstrated the presence of the tracer in the endocardium, in some endocytotic vesicles of subendothelial cells, probably macrophages, and between subendocardial myocytes up to 10 µm below the endocardial surface. Deeper into the subendocardial myocardium, tracer was not detected outside the coronary vessels. However, in the epicardium and subepicardial myocardium, 5 min after injection of LY-dextran 10000, tracer was observed in the interstitial tissue and in the extracellular spaces between myocytes (Fig. 6 F). *Ten min* after tracer injection ($n = 5$) there was general staining of interstitial tissue, deep into the myocardium of both ventricles. Fat tissue in the epicardium was intensively stained, and the yellow stain was sometimes visible with the naked eye. Staining of endocardial and myocardial interstitial tissue was now also visible on semithin plastic sections with epifluorescence microscopy (Fig. 7 A,7 B). Several cells, probably macrophages, loaded with heavily labeled vesicles were frequently seen in subendocardial and myocardial interstitial tissue. In rat hearts ($n = 3$) fixed 30 *min* after injection of LY-dextran 10000, tracer was observed only in these subendocardial and myocardial macrophages (Fig. 7 C).

In rat hearts ($n = 4$) fixed 1 or 10 min after intravenous injection of LY-dextran 40000, the tracer was not detected in endocardial and myocardial tissue of left or right ventricle with confocal scanning laser microscopy or with epifluorescence microscopy (Fig. 7 D).

In rat hearts ($n = 4$) fixed 1 to 2 min after intravenous injection of uncoupled Lucifer Yellow, the dye had penetrated rapidly both the EE and the endothelium of myocardial capillaries of left and right ventricle. Thick collagen fibers at the boundary of the endocardium and myocardium were heavily labeled (Fig. 8 A), and the connective tissue between myocytes was also stained (Fig. 8 B). Lucifer Yellow staining did not differ between epicardial and subendocardial myocardium.

Discussion

Structure of intercellular clefts in endocardial endothelium of rat heart

This study extends the structural investigation of junctional complexes of EE in rat heart (Anversa et al. 1973, 1975; Turcotte et al. 1982). No qualitative differences of the structure of intercellular clefts were noticed between EE of left and right ventricle. Regions of intercellular contact between EE cells frequently showed a complex interdigitation. Irregular and interdigitated intercellular clefts have also been reported in aortic endothelium (Huang et al. 1992). The estimated depth of "simple" and straightly sectioned clefts between two adjacent EE cells

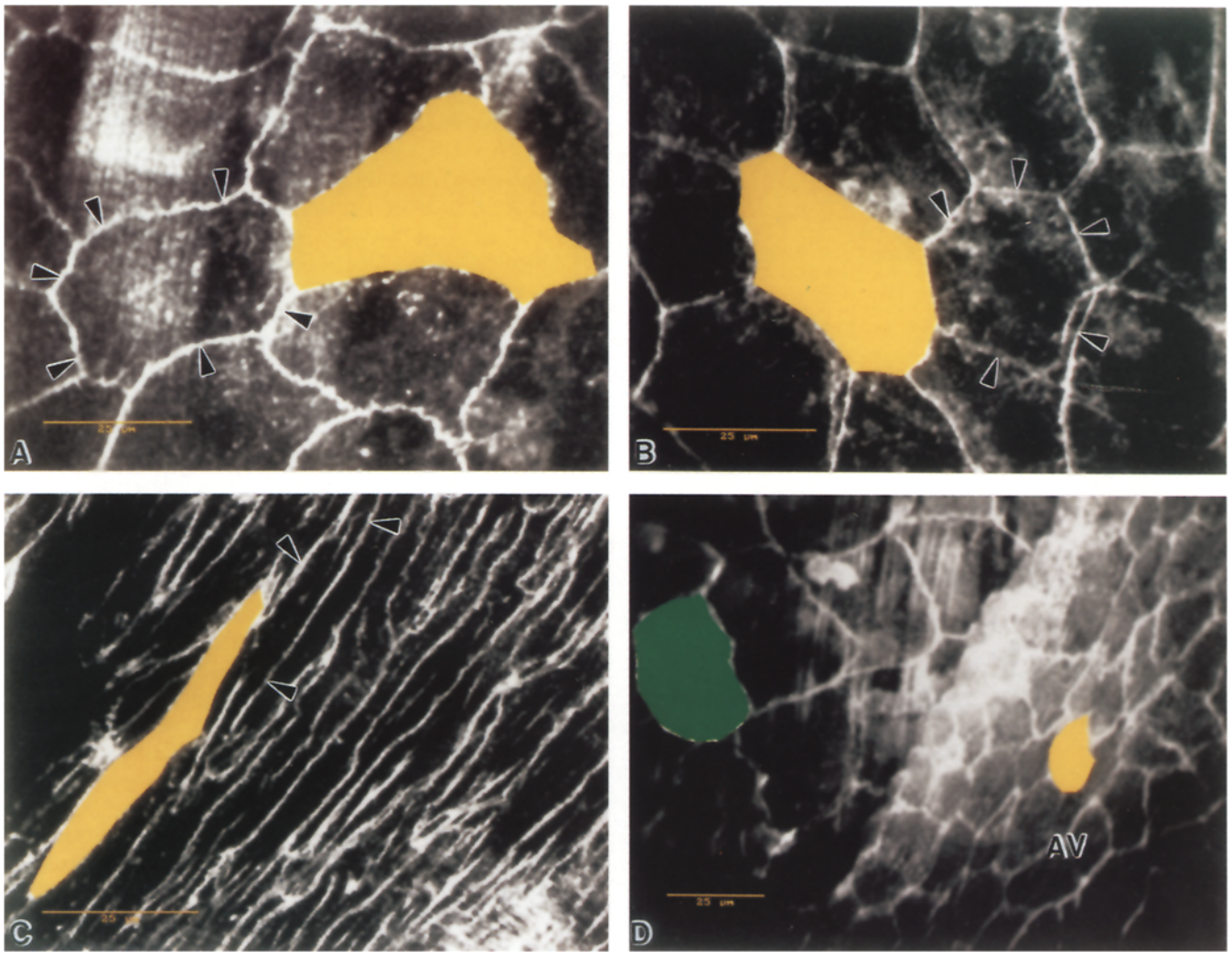

Fig. 5A–D. En face optical sections of endothelium stained with Bodipy-phallacidin. **A** Left ventricle, EE of a broad trabeculum from the apex. F-actin staining in EE cells is restricted to the peripheral actin band (*arrowheads*), which allows the measurement of cell area. EE cells in this zone are large (area 750 ± 20 μm^2; mean ± S.E.M., n = 30). The cell marked in yellow measures 990 μm^2. **B** Left ventricle, EE of papillary muscle. The surface area of the cell marked yellow measures 670 μm^2; the area of EE cells in this zone is 560 ± 20 μm^2 (mean ± S.E.M., n = 40). **C** Optical section through left ventricular myocardium. En face view of endothelium of an arteriole, which has a diameter of 200 μm. *Arrowheads* mark the peripheral band of an endothelial cell. Vascular endothelial cells are more elongated than EE cells and are usually smaller. The cell marked yellow measures 290 μm^2, the area of cells in this zone is 330 ± 10 μm^2 (mean ± S.E.M., n = 30). **D** Right ventricle. Thick optical section through EE and through endothelium of the atrioventricular valve (*AV*). EE cells (690 ± 20 μm^2; mean ± S.E.M., n = 30) are much larger than valvular endothelial cells (290 ± 20 μm^2; mean ± S.E.M., n = 60), which, especially, near the proximal border have a small surface area. The valvular cell marked yellow measures 150 μm^2. The EE cell marked green measures 730 μm^2

in rat was significantly larger than that between endothelial cells of myocardial capillaries (arithmetic mean: 0.53 μm; cf. 0.52 μm Bundgaard 1984).

Endocardial endothelial cells are large cells and have a different shape than vascular endothelial cells (Andries and Brutsaert 1993), which, therefore have longer intercellular clefts per unit endothelial cell surface area. The mean value obtained for aortic endothelium in our study was of the same magnitude as that reported for frog mesenteric capillary endothelium (Bundgaard and Frøkjaer-Jensen 1982).

Most junctional complexes in rat EE contained 1 or 2 junctional contact points, but a few intercellular clefts appeared devoid of any junctional contacts. In aortic endothelium, intercellular clefts free of junctions were suggested to provide the main route in transendothelial transport of macromolecules of the size of horseradish peroxidase (HRP) (Huang et al. 1992). A similar portion of open intercellular clefts has been reported for rat cardiac capillaries (Ward et al. 1988). However, goniometric tilting has shown that contact points which apparently obliterated the intercellular clefts were, in fact, areas where a narrow gap separated the two membranes (Ward et al. 1988). From these and other results (Bundgaard 1984; Curry and Michel 1980), it was suggested that the negatively charged fibrous matrix of the glycocalyx in the intercellular clefts might, to an important degree, influence endothelial permeability.

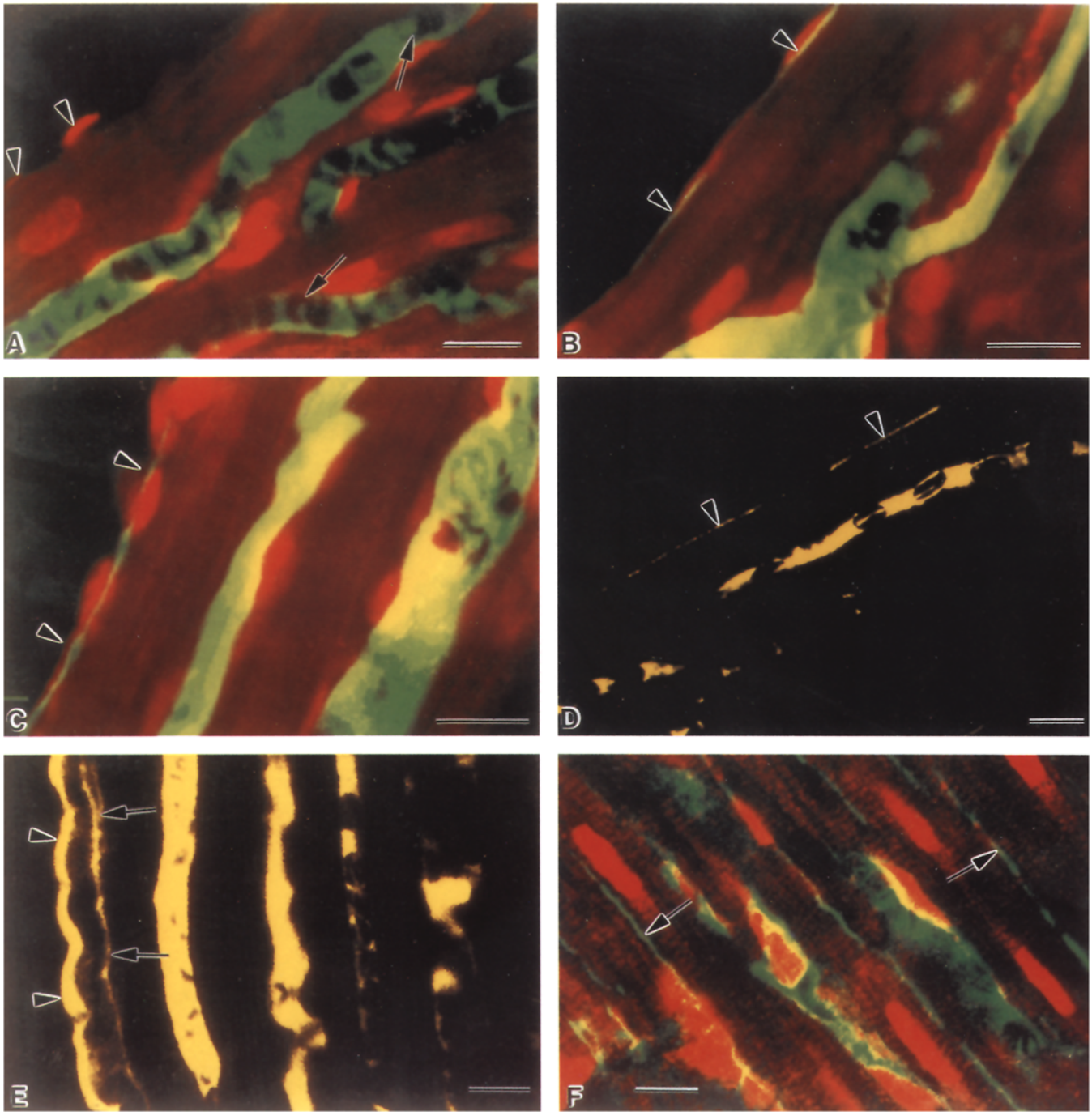

Fig. 6A–F. Confocal scanning laser optical sections through endocardium and myocardium of rat heart fixed at different time after intravenous injection of LY-dextran 10000. Red and green colored pictures (**A–C**, **F**) were obtained by merging the Lucifer Yellow image, of the FITC channel with the propidium iodide image from the rhodamine channel. Tissue in **A–C** and **D** was fixed with formaldehyde and glutaraldehyde, while tissue in **E** and **F** was fixed with formaldehyde solutions at different pH. **A** Heart fixed 60 s after injection. Right ventricle. No green colored tracer has penetrated the EE (*arrowheads*). In the red colored myocardium, green colored tracer is confined to the coronary vessels; note the presence of red blood cells (*arrows*). **B** Heart fixed 90 s after injection. Left ventricle. LY-dextran 10000 penetrated the EE (*arrowheads*) and stained subendocardial connective tissue; the tracer did not penetrate through the coronary vascular endothelium. **C** Heart fixed 120 s after injection, left ventricle; only the endocardium (*arrowheads*) was penetrated by LY-dextran 10000. **D** Heart fixed 120 s after injection, right ventricle; tissue was not counterstained with propidium iodide, so that the distribution of the yellow colored tracer is clearly visible in endo- and myocardium. LY-dextran 10000 is present only in the endocardium (*arrowheads*) and in the coronary vessels. **E** Heart fixed 5 min after injection, left ventricle; tissue was not counterstained with propidium iodide in order to show that tracer was visible only just below the EE (*arrowheads*) in the extracellular space between the first and second layer of myocytes (*arrows*) and in the coronary vessels. **F** Heart fixed 5 min after injection. In the epicardial myocardium, tracer was present in the interstitial tissue (*arrows*) between the myocytes. **A–F:** *Scale bars*: 10 μm

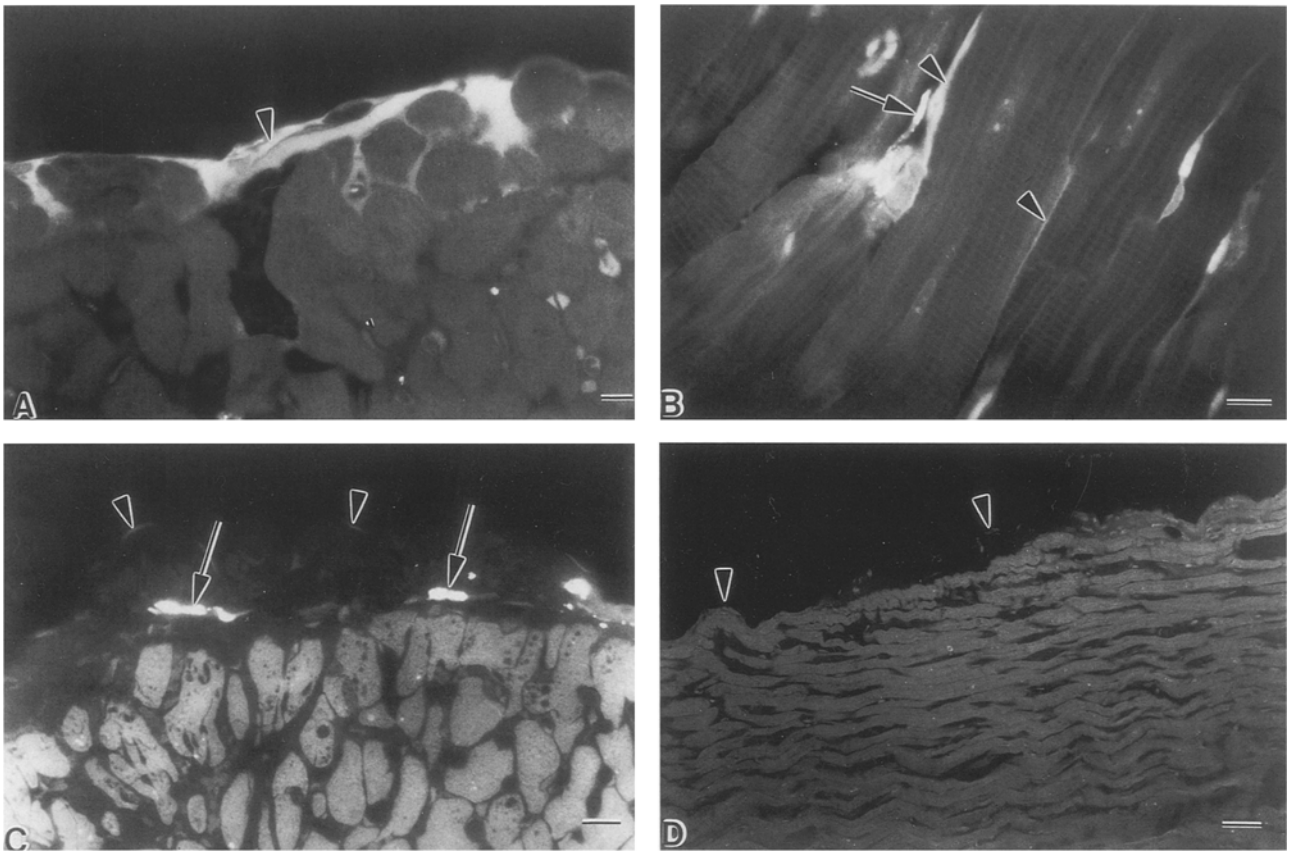

Fig. 7A–D. Semithin plastic sections of left ventricular wall observed with epifluorescence microscopy. Hearts were fixed 10 min (**A, B, D**) or 30 min (**C**) after injection of tracer. **A** LY-dextran 10000. Heavy subendocardial staining of connective tissue (*arrowhead*). *Scale bar*: 10 µm. **B** LY-dextran 10000. Myocytes deep in the myocardium are contoured by tracer (*arrowheads*). Macrophages contain heavily stained endocytotic vesicles (*arrow*). *Scale bar*: 10 µm. **C** LY-dextran 10000, 30 min after injection. Endocardial and myocardial interstitial tissue is not stained. Tracer is exclusively present in endocytotic vesicles of macrophages (*arrows*). *Arrowheads* indicate the EE. *Scale bar*: 10 µm. **D** LY-dextran 40000. No fluorescence is observed below the EE (*arrowheads*) or in the myocardium. *Scale bar*: 30 µm

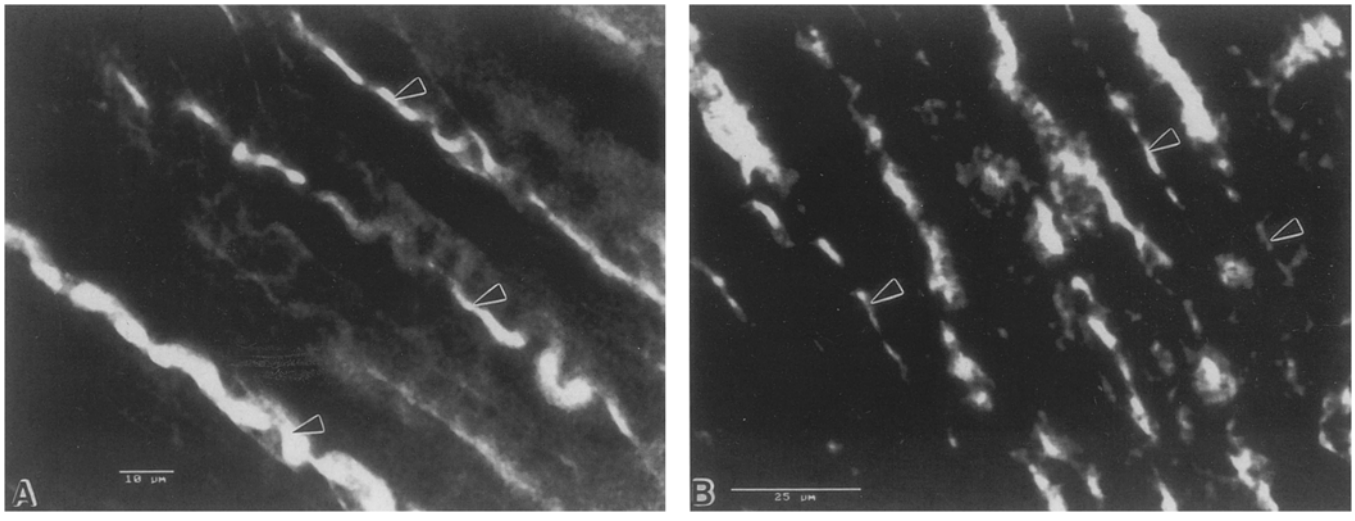

Fig. 8A, B. Optical sections with confocal scanning laser microscopy through heart tissue (left ventricle) fixed at 1 min after intravenous injection of unbound Lucifer Yellow. **A** Oblique en face section, partially below the EE (right side) showing labeling of thick, meandering collagen fibers (*arrowheads*) located at the junction between endocardium and myocardium. **B** Optical section through subendocardial myocardium demonstrating staining of interstitial tissue (*arrowheads*)

Intercellular junctions of EE are thus structurally similar to those of capillary vascular endothelium. However, the deep intercellular clefts between EE cells with the negatively charged glycocalyx and the low length of intercellular clefts per unit area in EE might diminish diffusion through the intercellular clefts, especially for negatively charged molecules like the anionic tracer used in the present study.

Permeability of EE in rat heart

The permeability experiments, however, showed the contrary. The EE was more permeable to LY-dextran 10000 than the coronary vascular endothelium. LY-dextran 40000 did not penetrate through the EE or through capillary endothelium, probably because of its larger molecular size.

One reason for the increased permeation through the EE could be the higher fluid pressure in the ventricular lumen than in the subendocardial myocardial capillaries. The fluorescent tracer penetrated the capillary endothelium in epicardial myocardium earlier than in subendocardial vessels. Permeation therefore accords with differences in fluid pressure, which is lower in subendocardial coronary vessels than in epicardial vessels (Rona et al. 1977). According to Starling's hypothesis (see Jain 1987; Michel 1992), transvascular transport is proportional to hydrostatic pressure. The ratio of transport driven by hydrostatic pressure (the socalled convective transport) to diffusional transport is expressed as the Peclet number (see Michel 1992). For large macromolecules, such as albumin, convection is responsible for 85% of the transport in skeletal muscle capillaries when fluid filtration rises to 5×10^{-5} $cm^3cm^{-2}s^{-1}$; hence, convective transport of these molecules is important. The Peclet number is less than 0.1 for molecules of less than 1 nm in radius and for smaller molecules transport by diffusion dominates (Michel 1992). The Stokes radius for LY-dextran 10000 has a value of 2 nm (Fig. 2 A) and thus, convective transport driven by a transmural pressure might be important for this molecule. By contrast, unbound Lucifer Yellow is much smaller and transport of such small molecules is driven by diffusional transport (Michel 1992). The rapid penetration of unbound Lucifer Yellow through subendocardial myocardial capillaries compared to the slower transendothelial transport of LY-dextran 10000 is thus compatible with the biophysical properties of the two tracers.

However, in the right ventricular wall, distribution of the fluorescent tracer was similar to that in the left ventricle, despite the lower filtration pressure. The techniques used in the present study might be not sensitive enough to detect differences in permeability between the ventricles. The signal from extra-vascular fluorescent tracer is dependent upon its concentration and its distribution in the interstitial tissue. The thickness of the interstitial tissue in the endocardium differs significantly between left and right ventricles and between different areas within the same ventricle (McMillan and Lev 1959). Without knowledge of the thickness of the endocardial layer and the concentration of the tracers in the interstitial tissue, interpretation of permeability between different zones of endocardium remains speculative.

Although EE appears to possess structural properties which limit paracellular diffusion, we cannot exclude the possibility that EE contains more open intercellular clefts, and is hence more permeable than capillary endothelium. Similarly, quantitative differences in the organization of tight junctions between left and right ventricle might explain the lack of observable dissimilarities in paracellular permeability between both ventricles. More ultrastructural studies are needed to elucidate the organization of tight junctions in EE.

The present tracer results probably confirm that net charge of the investigated molecules is important in paracellular permeability. LY-dextran 40000 did not penetrate through EE or through myocardial capillaries, whereas intravenously injected horseradish peroxidase (HRP; MW 40000) is known to diffuse rapidly through the subendocardial capillary endothelium (Anversa et al. 1973; Rona et al. 1977). Both molecules have a similar molecular weight, but the commonly used Type II HRP consists of a mixture of at least 2 isoenzymes with a different charge (Sibley et al. 1983). Positively charged HRP can penetrate a monolayer of cells more easily than negatively charged HRP (Sibley et al. 1983; Ward et al. 1988). The LY-dextrans used in the present study have a net negative charge and might thus possess different permeability properties from HRP. Interestingly, despite the high filtration pressure in the aorta, HRP did not penetrate across *open* intercellular clefts in aortic endothelium before 1 minute after intravenous injection (Huang et al. 1992). In contrast, HRP had already penetrated myocardial capillaries 8 seconds after injection and was visible in perivascular spaces (Anversa et al. 1973). This suggests that structural features, such as deeper and more complex intercellular clefts in aortic endothelium than in myocardial capillary endothelium, are important factors in transendothelial permeability.

In conclusion, the ultrastructure of EE might represent an adaptation to limit diffusion driven by the high hydrostatic pressure in the heart. The difference in transendothelial permeability between EE, capillary endothelium and perhaps other segments of coronary vessels like postcapillary venules, and lymphatic vessels, might establish characteristic diffusion properties of fluid and small solutes in endocardium and subjacent myocardium.

Acknowledgements. We are grateful to Drs. P. Verdijck and J. Meyers (University of Antwerp) for determining the physico-chemical properties of the fluorescent tracer.

References

Alexander JS, Hechtman HB, Shepro D (1988) Phalloidin enhances endothelial barrier function and reduces inflammatory permeability in vitro. Microvasc Res 35:308–315

Andries LA, Brutsaert DL (1993) Endocardial endothelium in the rat: cell shape and organization of the cytoskeleton. Cell Tissue Res 273:107–117

Anversa P, Giacomelli F, Wiener J, Spiro D (1973) Permeability properties of ventricular endocardium. Lab Invest 28:728–734
Anversa P, Giacomelli F, Wiener J (1975) Intercellular junctions of rat endocardium. Anat Rec 183:477–484
Berod A, Hartman BK, Pujol JF (1981) Importance of fixation in immunohistochemistry: use of formaldehyde solutions at variable pH for the localization of tyrosine hydroxylase. J Histochem Cytochem 29, 844–850
Brutsaert DL (1989) The endocardium. Annu Rev Physiol 51:263–273
Brutsaert DL, Andries LJ (1992) The endocardial endothelium. Am J Physiol 263:H985–H1002
Brutsaert DL, Meulemans AL, Sipido KR, Sys SU (1988) Effects of damaging the endocardial surface on the mechanical performance of isolated cardiac muscle. Circ Res 62:357–366
Bundgaard M (1980) Transport pathways in capillaries – In search of pores. Ann Rev Physiol 42:325–336
Bundgaard M (1984) The three-dimensional organization of tight junctions in a capillary endothelium revealed by serial-section electron microscopy. J Ultrastruct Res 88:1–17
Bundgaard M, Frøkjaer-Jensen J (1982) Functional aspects of the ultrastructure of terminal blood vessels: a quantitative study on consecutive segments of the frog mesenteric microvasculature. Microvasc Res 23:1–30
Cervos-Navarro J, Kannuki S, Nakagawa Y (1988) Blood-brain barrier (BBB). Review from morphological aspect. Histol Histopathol 3:203–213
Curry FE, Michel CC (1980) A fiber matrix model of capillary permeability. Microvasc Res 20:96–99
Gabbiani G, Badonnel MC, Rona G (1975) Cytoplasmic contractile apparatus in aortic endothelial cells of hypertensive rats. Lab Invest 32:227–234
Gimlich RL, Braun J (1985) Improved fluorescent compounds for tracing cell lineage. Develop Biol 109:509–514
Gotlieb AI, Langille L, Wong MKK, Kim DW (1991) Biology of disease. Structure and function of the endothelial cytoskeleton. Lab Invest 65:123–137
Huang A-L, Jan K-M, Chien S (1992) Role of intercellular junctions in the passage of horseradish peroxidase across aortic endothelium. Lab Invest 67:201–209
Jain RK (1987) Transport of molecules across tumor vasculature. Cancer Metastasis Rev 6:559–593
Li CX, Poznansky MJ (1990) Characterization of the ZO-1 protein in endothelial and other cell lines. J Cell Sci 97:231–237
McMillan JB, Lev M (1959) The aging heart. I. Endocardium. J Gerontol 14:268–283
Melax H, Leeson TS (1967) Fine structure of the endocardium in adult rats. Cardiovasc Res 1:349–355
Michel CC (1992) Capillary exchange. In: Seldin DW, Giebish G (eds) The kidney: physiology and pathophysiology. Raven Press, New York, pp 61–91
Pappenheimer JR, Renkin JR, Borrero LM (1951) Filtration, diffusion and molecular sieving through peripheral capillary membranes. A contribution to the pore theory of capillary permeability. Am J Physiol 167:13–46
Reynolds ES (1963) The use of lead citrate at high pH as an electron-opaque stain in electron microscopy. J Cell Biol 17:208–212
Rona G, Hüttner I, Boutet M (1977) Microcirculatory changes in myocardium with particular reference to catecholamine-induced cardiac muscle cell injury. In: Mussen H (ed) Handbuch der allgemeinen Pathologie III/7, Microzirkulation/Microcirculation. Springer, Berlin Heidelberg New York, pp 791–888
Schnittler HJ, Wilke A, Gress T, Suttorp N, Drenckhahn D (1990) Role of actin and myosin in the control of paracellular permeability in pig, rat and human vascular endothelium. J Physiol 431:379–401
Schulz R, Smith JA, Lewis MJ, Moncada S (1991) Nitric oxide synthase in cultured endocardial cells of the pig. Br J Pharmacol 104:21–24
Shasby DM, Shasby SS, Sullivan JM, Peach MJ (1982) Role of the endothelial cell cytoskeleton in control of endothelial permeability. Circ Res 51:657–661
Sibley CP, Bauman KF, Firth JA (1983) Molecular charge as a determinant of macromolecular permeability across the fetal capillary endothelium of the guinea-pig placenta. Cell Tissue Res 229:365–377
Simionescu M, Simionescu N, Palade G (1975) Segmental differentiation of cell junctions in the vascular endothelium. J Cell Biol 67:863–885
Smith JA, Shah AM, Lewis MJ (1991) Factors released from endocardium of the ferret and pig modulate myocardial contraction. J Physiol 439:1–14
Svensjö E, Grega GJ (1986) Evidence for endothelial cell-mediated regulation of macromolecular permeability by postcapillary venules. FASEB J 45:89–108
Tervo T, Joo A, Salminen L (1979) Penetration barrier to sodium fluorescein and fluorescein-labeled dextrans of various molecular sizes in brain capillaries. Experientia 35:252–255
Thorball N (1981) FITC-dextrans in microcirculatory and permeability studies using combined fluorescence stereo microscopy, fluorescence light microscopy and electron microscopy. Histochemistry 71:209–233
Turcotte H, Bazin M, Boutet M (1982) Junctional complexes in regenerating endocardium. J Ultrastruct Res 79:133–141
Ward BJ, Bauman KF, Firth JA (1988) Interendothelial junctions of cardiac capillaries in rats: their structure and permeability properties. Cell Tissue Res 252:57–66